Successive Stripe Artifact Removal Based on Robust PCA for Millimeter Wave Automotive Radar Image

Weiwei SHAN*, Shogo MURAMATSU†, Akira OSHIMA* and Hiroyoshi YAMADA†
* Graduate School of Science and Technology, Niigata Univ., Niigata, Japan
† Faculty of Engineering, Niigata Univ., Niigata, Japan
E-mail: shogo.muramatsu.jp@ieee.org

***Abstract*—This study proposes a stripe artifact removal method based on robust principal component analysis (RPCA) for millimeter wave (MW) automotive radar images. With the development of MW radar detection technology, there is a demand for installing obstacle detectors on vehicular for safety. From this background, the authors developed squint-mode synthetic aperture radar (SAR) with MW (MW-SAR) as a high-resolution imaging technique. For synthesizing radar images, a back-projection algorithm (BPA) is adopted because of its real-time processing nature with high accuracy. However, SAR images obtained with Single Input and Single Output (SISO) systems are prone to be contaminated by a stripe-shaped artifact and can affect to the obstacle detection performance. Thus, to reduce the structured noise, this paper proposes successive RPCA on the assumption that the stripe artifacts and obstacle reflection are low-rank and sparse, respectively. As a solver, the alternating direction method of multipliers (ADMM) is adopted. The main contribution of this work is to initialize the ADMM state by taking account of the similarity of low-rank components between adjacent segments. Through simulations with experimental data, the significance of the proposed method is verified.**

I. Introduction

With the rapid growth of artificial intelligence technology and the formation of the intelligent transportation industry, the advanced driver-assistance systems (ADAS) are gradually attracting people's attention. In this situation, robust detection of obstacles has become one of the important research directions. Unlike optical cameras and infrared radars, millimeter wave (MW) radar has advantages of high accuracy, long detection distance and high resistance to bad weather such as rain, fog and snow. As a result, MW radar becomes an indispensable element of ADAS [1]. From this background, we are developing a squint-mode synthetic aperture radar (SAR) with MW (MW-SAR) as a high-resolution imaging technique [2], [3]. For the automotive applications, the main purpose is to detect objects on the front side. When an object such as a pedestrian crossing ahead exists, the synthesis should be performed up to the position. Unlike the air-borne and space-borne SAR, the real-time capability is of interest.

In order to realize the online synthesis aperture, we adopt a back-projection algorithm (BPA) [4]. BPA has advantages in the real-time processing compared with the competitive beam forming and in the high accuracy compared with the competitive range Doppler method. However, SAR images obtained by BPA with simple Single Input and Single Output (SISO) systems are prone to be contaminated by stripe-shaped artifacts, which can affect to the obstacle detection performance. The synergetic effect of the reconstruction and correlated clutter causes stripe-shaped artifacts as structural noise. The stripe artifacts in SAR images can degrade the obstacle detection performance after the acquisition. To overcome this degradation, one approach is to adopt a Single Input and Multiple Output (SIMO) radar system, which the authors proposed before [5]. In this work, as another approach, we develop a computational method to remove the stripe artifacts for SIMO MW-SAR systems.

SAR systems acquire high-resolution images. Therefore, the restoration solver should be simple, and further be effective for the target problem. The stripe artifacts have regular structure and can be assumed to have low rank when viewed as matrices. With an additional assumption that significant obstacles are sparsely located, we can reduce the stripe artifact removal problem to robust principal component analysis (RPCA, Robust PCA) [6]. RPCA is proposed by Wright *et al.* and gives us a two term representation of a data matrix as the sum of low rank and sparse matrix.

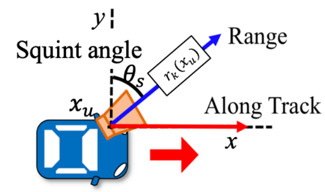

Fig. 1. Observation model of automotive MW-SAR imaging

By using the RPCA formulation, we propose to decompose a contaminated SAR image into stripe artifact and significant obstacles. Through the convex-relaxation, the problem becomes able to be solved by the alternating direction method of multipliers (ADMM). As a result, a simple solver can be obtained. However, the algorithm must consider real-time capability. Therefore, we propose to divide a SAR image into small segments in the azimuth direction, and remove the stripe artifacts segment by segment. Since ADMM requires iterative process, an appropriate initial state must be set in order to reduce the number of iterations. As an online initialization method, we further propose to successively transfer the state of the previous segment to the current one. We apply this method to the stripe artifacts removal from MW-SAR images and verify the significance of the proposed method through simulations with experimental data.

II. Overview of MW-SAR Data Acquisition

This section provides an overview of MW-SAR observation model and discusses the causes of stripe artifacts.

A. SAR Imaging Algorithm

SAR imaging is a method in which the radar detects objects while moving, and then the result is synthesized with high precision to virtually generate a large-aperture antenna. Fig. 1 shows the geometry of the observation model for the automotive MW-SAR system that we deal with [7]. The SAR imaging algorithm of this study is based on BPA [4]. In Fig. 1, we suppose the x-axis is the moving direction and $\theta_{\rm s}$ represents the squint angle. We employ the Linear-FM (LFM)

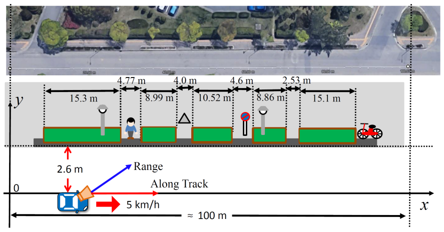

Fig. 2. Experimental setup for automotive MW-SAR imaging

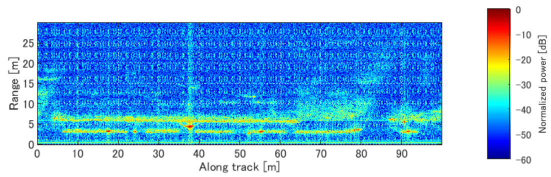

(a)

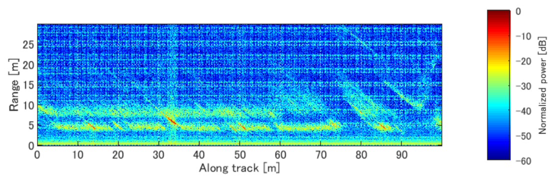

(b)

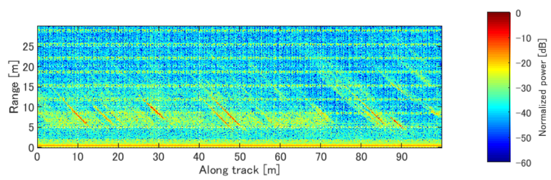

(c)

Fig. 3. Magnitudes of SISO MW-SAR images of different squint angles, where (a) $\theta_s = 0°$, (b) $\theta_s = 45°$ and (c) $\theta_s = 70°$.

radar, and a SAR image is reconstructed by

$$P_{\mathrm{BPA}}(x, y) = \frac{1}{N}\sum_{N} s_{\mathrm{b}}(x, y, x_{\mathrm{u}}) \exp\left(-j\frac{4\pi f_{\mathrm{c}}}{c} r(x, y, x_{\mathrm{u}})\right), \tag{1}$$

where x and y are positions in the along track (azimuth) and range direction, respectively, N is the number of observation points, $r(x, y, x_{\mathrm{u}})$ is the range distance between the antenna position $x = x_{\mathrm{u}}$ and observation point (x, y), and $s_{\mathrm{b}}(x, y, x_{\mathrm{u}})$ is the image created by mapping a range data on the beat-spectrum at x_{u}, f_{c} is the center frequency and c is the speed of light [7].

B. Stripe Artifacts

Fig. 2 shows an experimental setup for measuring environment with an automotive MW-SAR system, and Fig. 3 shows SISO MW-SAR results with squint angles of 0°, 45° and 70°, where the specification is summarized in Section IV. From the images shown in Fig. 3, it is observed that the SISO MW-SAR results have significant interference with stripe shape along track. In order to detect obstacles ahead quickly, the squint angle θ_s should be close to 90°. However, the stripe artifacts are getting stronger as θ_s increases. The mechanism of causing the interference have not been analyzed exactly. Our conjecture is that it is due to insufficient interval of sampling in the azimuth direction, and the synergetic effect of the reconstruction and correlated clutter causes the structural noise.

III. Stripe Artifact Removal with RPCA

In this section, we propose to apply RPCA to reduce the stripe artifacts in SISO MW-SAR images on the assumption that an observation is composed of a stripe artifact and obstacle reflection component, and the former is low-rank and the latter is sparse, respectively. As a solver, ADMM is successively adopted to small segments with initialization by taking account of the similarity of low-rank components between adjacent segments.

A. Assumption

Let $\mathbf{M} \in \mathbb{C}^{M\times K}$ is an observation matrix of MW-SAR image, where $M \in \mathbb{N}$ and $K \in \mathbb{N}$ are the numbers of rows and columns, respectively. From the regular structure of the stripe artifacts, we can expect some dependencies on the structural noise, i.e., the low rank property as a matrix.

Therefore, we assume that the observation $\mathbf{M}$ can be decomposed into two components as

$$\mathbf{M} = \mathbf{L} + \mathbf{S}, \tag{2}$$

where $\mathbf{L} \in \mathbb{C}^{M\times K}$ is a low-rank component and $\mathbf{S} \in \mathbb{C}^{M\times K}$ is a sparse component. We expect that $\mathbf{L}$ consists of the stripe artifacts and $\mathbf{S}$ consists of the obstacle reflections. The goal of our image restoration is to remove $\mathbf{L}$ from $\mathbf{M}$. Thus, $\mathbf{S}$ is what we demand.

B. Robust Principal Component Analysis

Let us formulate the decomposition problem in (2). We propose to use RPCA to separate the observation $\mathbf{M}$ into the stripe artifacts $\mathbf{L}$ and the obstacle reflections $\mathbf{S}$.

1) Problem Formulation: RPCA is a signal processing method based on compressed sensing [8] and sparse expression theory [**?**]. The core idea of RPCA is to decompose the contaminated observation matrix $\mathbf{M}$ into a low rank matrix $\mathbf{L}$ and a sparse matrix $\mathbf{S}$ by an optimization criterion with the rank of $\mathbf{L}$ regularized by the sparsity of $\mathbf{S}$ under the constraint of (2).

We formulate the SAR image restoration problem as

$$\min_{\mathbf{L},\mathbf{S}\in\mathbb{C}^{M\times K}} \operatorname{rank}(\mathbf{L}) + \lambda\|\mathbf{S}\|_0 \quad \text{s.t.} \quad \mathbf{L} + \mathbf{S} = \mathbf{M}, \tag{3}$$

where $\operatorname{rank}(\cdot)$ denotes the rank of the argument, $\|\cdot\|_0$ denotes the ℓ_0 pseudo norm, which counts the number of nonzero entries, and $\lambda > 0$ is a regularization parameter.

2) Convex Relaxation: It is known that the problem in (3) is NP-hard and thus numerically intractable. Therefore, we apply the convex relaxation to (3) so that we can approximately solve it as a convex optimization problem. Let us modify (3) to a convex optimization problem as

$$\min_{\mathbf{L},\mathbf{S}\in\mathbb{C}^{M\times K}} \|\mathbf{L}\|_* + \lambda\|\mathbf{S}\|_1 \quad \text{s.t.} \quad \mathbf{L} + \mathbf{S} = \mathbf{M}, \tag{4}$$

where $\|\cdot\|_*$ denotes the nuclear norm, i.e., the sum of the singular values, and $\|\cdot\|_1$ denotes the ℓ_1 norm, i.e., the sum of the absolute values of all elements in the matrix.

C. Alternating Direction Method of Multipliers (ADMM)

(4) is a convex optimization problem and has the global optimal solution. Glowinski *et al.* proposed ADMM [10], which gives a computational framework for solving a certain form of convex optimization problems. ADMM breaks down a large global problem into multiple small easy-to-resolve local small problems, and adjusts the small problem solutions to solve the large global problems. It is suitable for solving distributed convex optimization problems.

Algorithm 1 ADMM for solving Problem (4)

Input: $\mathbf{Z}_i^{(0)}$, $\mathbf{D}_i^{(0)}$ for $i \in \{1,2,3\}$, $\rho > 0$, $n = 0$
Output: $\mathbf{L}^{(n)}$, $\mathbf{S}^{(n)}$

1: **while** a stopping criterion is not satisfied, **do**
2: $\mathbf{L}^{(n+1)} := \frac{1}{3}\left(2\mathbf{Z}_1^{(n)} - 2\mathbf{D}_1^{(n)} - \left(\mathbf{Z}_2^{(n)} - \mathbf{D}_2^{(n)}\right) + \mathbf{Z}_3^{(n)} - \mathbf{D}_3^{(n)}\right)$
3: $\mathbf{S}^{(n+1)} := \mathbf{Z}_1^{(n)} - \mathbf{D}_1^{(n)} + \mathbf{Z}_3^{(n)} - \mathbf{D}_3^{(n)} - 2\mathbf{L}^{(n+1)}$
4: $\mathbf{Z}_1^{(n+1)} := \mathrm{prox}_{\frac{1}{\rho}\|\cdot\|_*}\left(\mathbf{L}^{(n+1)} + \mathbf{D}_1^{(n)}\right)$
5: $\mathbf{Z}_2^{(n+1)} := \mathrm{prox}_{\frac{\lambda}{\rho}\|\cdot\|_1}\left(\mathbf{S}^{(n+1)} + \mathbf{D}_2^{(n)}\right)$
6: $\mathbf{Z}_3^{(n+1)} := \mathrm{prox}_{\frac{1}{\rho}\iota_{\{\mathbf{M}\}}}\left(\mathbf{L}^{(n+1)} + \mathbf{S}^{(n+1)} + \mathbf{D}_3\right)$
7: $\mathbf{D}_1^{(n+1)} := \mathbf{D}_1^{(n)} + \mathbf{L}^{(n+1)} - \mathbf{Z}_1^{(n+1)}$
8: $\mathbf{D}_2^{(n+1)} := \mathbf{D}_2^{(n)} + \mathbf{S}^{(n+1)} - \mathbf{Z}_2^{(n+1)}$
9: $\mathbf{D}_3^{(n+1)} := \mathbf{D}_3^{(n)} + \mathbf{L}^{(n+1)} + \mathbf{S}^{(n+1)} - \mathbf{Z}_3^{(n+1)}$
10: $n \leftarrow n+1$
11: **end while**

1) RPCA with ADMM: (4) is a typical convex optimization problem, but it is difficult to be solved directly. By incorporating the indicator function $\iota_C(\cdot)$ for a closed convex set C, we can equivalently rewrite the problem as in the following unconstrained minimization problem:

$$\min_{\mathbf{L},\mathbf{S}\in\mathbb{C}^{M\times K}} \|\mathbf{L}\|_* + \lambda\|\mathbf{S}\|_1 + \iota_{\{\mathbf{M}\}}(\mathbf{L}+\mathbf{S}). \tag{5}$$

The problem in (5) has a form which can be solved by ADMM. The algorithm is derived as in Algorithm 1, where the proximal operators $\mathrm{prox}_{\gamma\|\cdot\|_*}(\cdot)$, $\mathrm{prox}_{\gamma\|\cdot\|_1}(\cdot)$ and $\mathrm{prox}_{\gamma\iota_C}(\cdot)$ are expressed for $\gamma > 0$ as follows:

$$\mathrm{prox}_{\gamma\|\cdot\|_*}(\mathbf{X}) := \mathbf{U}\mathcal{S}_\gamma(\mathbf{\Sigma})\mathbf{V}^{\mathsf{H}}, \tag{6}$$

$$\mathrm{prox}_{\gamma\|\cdot\|_1}(\mathbf{X}) := \mathcal{S}_\gamma(\mathbf{X}), \tag{7}$$

$$\mathrm{prox}_{\gamma\iota_{\{\mathbf{M}\}}}(\mathbf{X}) := P_{\{\mathbf{M}\}}(\mathbf{X}) = \mathbf{M}, \tag{8}$$

where $\mathbf{U} \in \mathbb{C}^{M\times r}$ and $\mathbf{V} \in \mathbb{C}^{K\times r}$ are unitary matrices and $\mathbf{\Sigma} \in \mathbb{R}^{r\times r}$ is a diagonal matrix consisting of r singular values of the matrix $\mathbf{X} \in \mathbb{C}^{M\times K}$, which are obtained by the singular decomposition

$$\mathbf{X} = \mathbf{U}\mathbf{\Sigma}\mathbf{V}^{\mathsf{H}}. \tag{9}$$

The superscript H denotes the Hermitian transposition. In addition, $\mathcal{S}_\gamma(\cdot)$ is the element-wise soft-thresholding function defined by

$$[\mathcal{S}_\gamma(\mathbf{X})]_{m,k} := [\mathbf{X}]_{m,k} \cdot \max\left(1 - \gamma/\left|[\mathbf{X}]_{m,k}\right|, 0\right), \tag{10}$$

where $[\cdot]_{m,k}$ denotes the m-th row and k-th column element, and $P_C(\cdot)$ is a metric projection to a closed convex set $C \subset \mathbb{C}^{M\times K}$.

2) Initialization: Before running Algorithm 1, we need to initialize the states $\mathbf{Z}_i^{(0)}$ and $\mathbf{D}_i^{(0)}$ for $i \in \{1,2,3\}$. We can start $\mathbf{L}^{(1)} = \mathbf{M}$ and $\mathbf{S}^{(1)} = \mathbf{O}_{M\times K}$ by using the following setup:

$$\begin{aligned} &\mathbf{Z}_1^{(0)} = \mathbf{M}, && \mathbf{Z}_2^{(0)} = \mathbf{O}_{M\times K}, && \mathbf{Z}_3^{(0)} = \mathbf{M}, \\ &\mathbf{D}_1^{(0)} = \mathbf{O}_{M\times K}, && \mathbf{D}_2^{(0)} = \mathbf{O}_{M\times K}, && \mathbf{D}_3^{(0)} = \mathbf{O}_{M\times K}, \end{aligned}$$

where $\mathbf{O}_{M\times K}$ denotes the zero matrix of size $M \times K$.

D. Online Initialization for Successive RPCA

It should be noted that automotive MW-SAR imaging requires real-time processing. Therefore, it is preferable to reduce the number of iterations in ADMM. In addition, it is necessary to remove stripe artifacts successively moment by moment. For these demands, we propose to partially process small segments of the SAR image and initialize each ADMM state by taking account of the similarity of low-rank components between adjacent segments.

TABLE I
EXPERIMENTAL SETUP

Radar system	Linear FM-CW
Center frequency	76.5 GHz
Frequency bandwidth	0.9 GHz
Sweep time	0.5 msec.
Sampling frequency	1.2 msec.
Pulse reputation interval	5 km/h
SAR method	Backprojection method
Squint angle	0°, 45°, 70°

Let $\mathbf{M}_p \in \mathbb{C}^{M\times K}$ be the p-th SAR observation and M be a time-series data of those observations as

$$\mathsf{M} = \{\mathbf{M}_0, \mathbf{M}_1, \mathbf{M}_2, \cdots\}. \tag{11}$$

The stripe artifacts removal is separately performed for each segment. Since the process is divided in the azimuth direction, we propose to initialize the ADMM states $\mathbf{Z}_i$ and $\mathbf{D}_i$ for $i \in \{1,2,3\}$ by using the state of the previous segment except for the constraint regarding with the observation as $\mathbf{Z}_3 = \mathbf{M}_p$.

Let $\mathbf{Z}_{p,i}$ and $\mathbf{D}_{p,i}$ for $i \in \{1,2,3\}$ be variables $\mathbf{Z}_i$ and $\mathbf{D}_i$ in Algorithm 1 for the p-th segment $\mathbf{M}_p$, respectively. Then, we propose to initialize those state variables from the previous segment except for $\mathbf{Z}_{p,3}$ as follows:

a) For $p = 0$:

$$\begin{aligned} &\mathbf{Z}_{p,1}^{(0)} = \mathbf{M}_p, && \mathbf{Z}_{p,2}^{(0)} = \mathbf{O}_{M\times K}, && \mathbf{Z}_{p,3}^{(0)} = \mathbf{M}_p, \\ &\mathbf{D}_{p,1}^{(0)} = \mathbf{O}_{M\times K}, && \mathbf{D}_{p,2}^{(0)} = \mathbf{O}_{M\times K}, && \mathbf{D}_{p,3}^{(0)} = \mathbf{O}_{M\times K}, \end{aligned}$$

b) For $p > 0$:

$$\begin{aligned} &\mathbf{Z}_{p,1}^{(0)} = \mathbf{Z}_{p-1,1}^{(\mathrm{end})}, && \mathbf{Z}_{p,2}^{(0)} = \mathbf{Z}_{p-1,2}^{(\mathrm{end})}, && \mathbf{Z}_{p,3}^{(0)} = \mathbf{M}_p, \\ &\mathbf{D}_{p,1}^{(0)} = \mathbf{D}_{p-1,1}^{(\mathrm{end})}, && \mathbf{D}_{p,2}^{(0)} = \mathbf{D}_{p-1,2}^{(\mathrm{end})}, && \mathbf{D}_{p,3}^{(0)} = \mathbf{D}_{p-1,3}^{(\mathrm{end})}. \end{aligned}$$

The superscript (end) represents the final state of ADMM.

IV. PERFORMANCE EVALUATION

This section evaluates the performance of the proposed stripe artifact removal method. We compare the results of RPCA with different initialization methods for experimental MW-SAR images acquired by a SISO system.

A. Experimental Setup

Stripe artifact removal is performed for data acquired by an actual SISO MW-SAR system. Fig. 3 shows magnitudes of three SAR images acquired with different squint angles, i.e., $\theta_\mathrm{s} \in \{0^\circ, 45^\circ, 70^\circ\}$. The environmental setup is shown in Fig. 2 and the specifications on the experimental system setup are summarized in Table I. Every image is normalized with each maximum value. The dimension is 60000 lines in the azimuth direction and 219 points in the range direction.

B. Experimental Results

Each time series image shown in Fig. 3 was divided into 100 segments of size $M\times K = 219\times 600$ as $\mathsf{M} = \left\{\mathbf{M}_p \in \mathbb{C}^{219\times 600}\right\}_{p=0}^{99}$, where the dimension of $\mathbf{M}_p$ corresponds to around 30m in the range direction and around 1m along track. Each segment is processed sequentially from 0m to 100m along track.

Fig. 4 (a) and (b) show the restoration results of $\theta_\mathrm{s} = 45^\circ$ and $\theta_\mathrm{s} = 70^\circ$ by the independent initialization of ADMM, respectively, and Fig. 5 (a) and (b) show those by using the proposed online initialization method. The top and bottom images show the

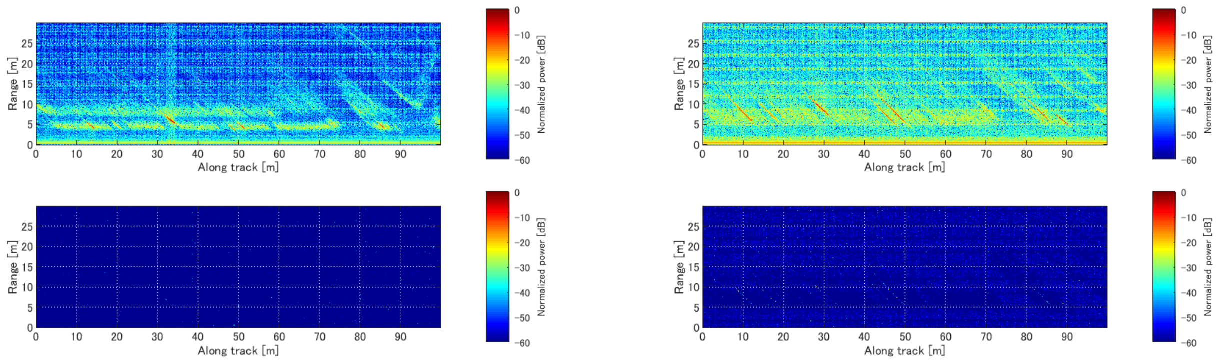

(a) (b)

Fig. 4. Results of independent initialization, where the top and bottom images are magnitudes of low-rank component L and sparse component S, respectively. (a) $\theta_{\mathrm{s}} = 45°$, (b) $\theta_{\mathrm{s}} = 70°$,

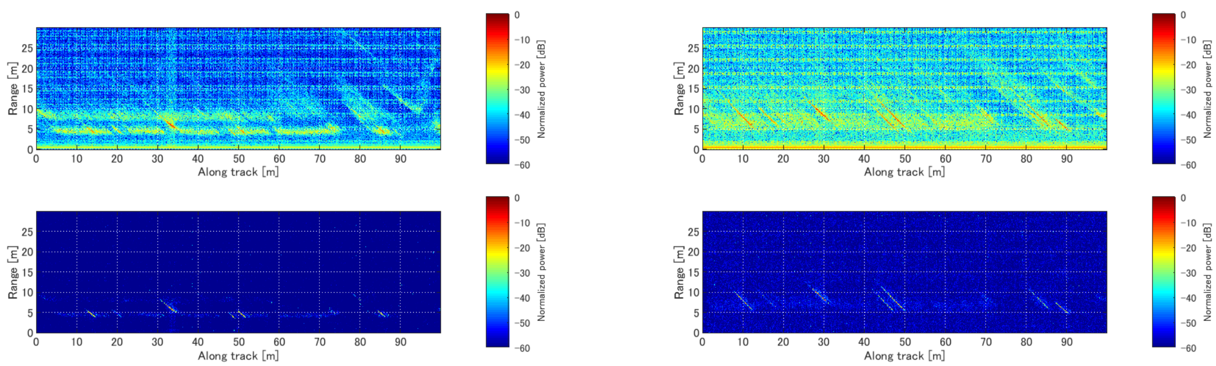

(a) (b)

Fig. 5. Results of proposed online initialization, where the top and bottom images are magnitudes of low-rank component L and sparse component S, respectively. (a) $\theta_{\mathrm{s}} = 45°$, (b) $\theta_{\mathrm{s}} = 70°$,

TABLE II
CONFIGURATIONS OF ADMM

$M \times K$	λ	ρ	♯iterations
219×600	0.1	1.0	10

magnitudes of low-rank component $\mathsf{L} = \left\{\mathbf{L}_p \in \mathbb{C}^{219\times600}\right\}_{p=0}^{99}$ and sparse component $\mathsf{S} = \left\{\mathbf{S}_p \in \mathbb{C}^{219\times600}\right\}_{p=0}^{99}$, respectively, where $\mathbf{M}_p = \mathbf{L}_p + \mathbf{S}_p$, and all data are normalized with the original maximum value. Table II summarizes the configurations of ADMM.

The restoration image appears as the sparse component S. Note that the number of iterations are set to 10 for every case. It is clear that the proposed online initialization emphasizes obstacles and performs better than the independent initialization.

V. CONCLUSION

In this study, we proposed to apply RPCA to SISO MW-SAR image restoration. A successive stripe artifact removal algorithm is proposed based on ADMM. From some experimental results, the significance of our proposed method was verified through comparison with the traditional ADMM approach. In the future, we will further study the cause of the artifacts, refine the model and improve the restoration performance.

ACKNOWLEDGMENT

This work was partly supported by the JSPS KAKENHI Grant number 17H03261 and 19H04135, Japan.

REFERENCES

[1] J. Minotani, H. Yamada, Y. Yamaguchi, and Y.Sugiyama,“Fundamental study on synthetic aperture radar imaging by using millimeter wave automotive radar,” vol. 115, pp. 37-42, Aug 2015.

[2] J. Minotani, H. Yamada, and Y. Yamaguchi, “Experimental study on MW-SAR imaging in outdoor environment,” *2015 International Workshop on Electromagnetics: Applications and Student Innovation Competition (iWEM),* pp. 1-2, Nov 2015.

[3] Mehrdad and Soumekh, “Synthetic aperture radar signal processing,” *New York: Wiley,* vol. 7, 1999.

[4] A. Ribalta, “Time-domain reconstruction algorithms for fmcw-sar,” *IEEE Geoscience and Remote Sensing Letters,* vol. 8, no. 3, pp. 396-400, May 2011.

[5] A. Oshima, H. Yamada, Y. Yamaguchi, and S. Muramatsu, “Fundamental study on ambiguity suppression of automotive squint-mode MW-SAR by using SIMO radar,” pp. 1-2, Aug 2018.

[6] J. Emmanuel, J. Candes, X. Li, Y. Ma, and J.Wright, “Robust principal component analysis?,” *Journal of the ACM (JACM),* vol. 58, pp. 68-73, May 2011.

[7] T. Kobayashi, H. Yamada, Y. Sugiyama, S. Muramatsu, and Y. Yamagchi, “Study on imaging method and doppler effect for millimeterwave automotive sar,” *2018 International Symposium on Antennasand Propagation (ISAP),* pp. 1-2, Oct 2018.

[8] Donoho and L. David, “Compressed sensing,” *IEEE Transactions onInformation Theory,* vol. 52, pp. 1289-1306. Apr 2016.

[9] E. Michael, “Sparse and redundant representations: From theory to applications in signal and image processing.” *Springer-Verlag New York,* no. 1, pp. 1-376, Jul 2010.

[10] S. Boyd, N. Parikh, E. Chu, B. Peleato, and J. Eckstein, “Distributed optimization and statistical learning via the alternating direction method of multipliers,” *Foundations and Trends in Machine Learning,* vol. 3, pp. 1-70, Jul 2011.